Systematic study of the electronic state in θ-type BEDT-TTF organic conductors by changing the electronic correlation

Hatsumi Mori and Shoji Tanaka
International Superconductivity Technology Center, Superconductivity Research Laboratory, 1-10-13 Shinonome Koto-ku Tokyo 135, Japan

Takehiko Mori
Department of Organic and Polymeric Materials, Tokyo Institute of Technology, O-okayama, Meguro-ku Tokyo 152, Japan

(Received 25 June 1997; revised manuscript received 10 November 1997)

The behavior of the phase transitions is mapped out as a function of the dihedral angle (θ) or the transfer integral (t) between donor columns for θ-type BEDT-TTF [BEDT-TTF: bis(ethylenedithio)tetrathiafulvalene, abbreviated as ET] salts involving the series θ-(BEDT-TTF)$_2MM'$(SCN)$_4$ [M=Tl,Rb,Cs, M'=Co,Zn: abbreviated as θ-MM'], which we have recently prepared. The electronic correlation parameter (U/t) increases by increasing the dihedral angle (θ). In the phase diagram of θ-ET salts the ground state varies from insulating, to superconducting, to metallic with decreasing θ, namely, U/t. The series θ-MM' is located at the center of the phase diagram where metallic, paramagnetic insulating, and singlet states are observed at low temperatures. With applied pressure, the metal-insulator transition temperature rises because the dihedral angle increases, which is related to the enhancement of the electronic correlation. [S0163-1829(98)03919-8]

INTRODUCTION

It has been widely accepted that intermolecular overlap integrals of HOMO of donor molecules, which are calculated by the extended Huckel method, and band structure calculated using transfer integrals by assuming the tight-binding model, are important tools for understanding the electronic states of organic conductors.[1] Empirically the Fermi surface (FS) has been determined by Shubnikov–de Haas, de Haas–van Alphen effects, and angular dependence of magnetoresistance oscillation (AMRO),[2] which is in agreement with the calculated FS. However, the highly correlated system is the exception. Though the calculation gives one- or two-dimensional FS, some salts are magnetic insulators even at room temperature; for example, α'-ET$_2$AuBr$_2$ [ET=BEDT-TTF],[3(a)] β'-ET$_2$ICl$_2$,[3(b)] γ'-ET$_2$AuI$_2$,[3(c)] θ-ET$_4$Hg$_3$I$_8$,[4(a)] θ-ET$_2$Cu$_2$(CN)[N(CN)$_2$]$_2$,[4(b)] θ-ETAgBr$_3$,[4(c)] θ-ETAg$_x$(SCN)$_2$,[4(d)] θ-ETCd$_{0.66}$(SCN)$_2$,[4(e)] and θ-ET$_2$TlZn(SCN)$_4$.[4(f)] In particular, θ-type BEDT-TTF salts are mysterious, because they afford a wide variety of electronic states from insulators to a superconductor, θ-ET$_2$I$_3$ with T_c=3.6 K.[5] Recently we have prepared the series θ-(BEDT-TTF)$_2MM'$(SCN)$_4$ [M=Tl,Rb,Cs, M'=Co,Zn]. The crystal structure of θ-(BEDT-TTF)$_2$RbZn(SCN)$_4$ is shown in Fig. 1. The thick anion sheet of 8.1 Å and the donor layer stack alternately along the b axis [Fig. 1(a)] in the anion sheet, Zn^{2+}, is coordinated by four N atoms of NCS^- tetrahedrally and Rb^+ is surrounded ionically by eight S atoms of SCN^- to construct a two-dimensional anion network [Fig. 1(b)]. The BEDT-TTF molecules form the θ-type donor arrangement. The donor stacks regularly and the calculated transverse transfer integral (t_p) is larger than the stacking one (t_c). The calculated FS is two-dimensional [Figs. 1(c) and 1(d)]. The metal-insulator transitions of θ-(BEDT-TTF)$_2MM'$(SCN)$_4$ [M=Tl,Rb,Cs, M'=Co,Zn] have been observed between 20 and 250 K. The θ-MM' series is located between the insulating and metallic θ phases, filling a gap in the phase diagram and enabling us to understand the electronic states of θ-type BEDT-TTF salts by a unified phase diagram as a function of electronic correlation parameter, U/t.

In this paper, the electrical resistivity and thermoelectric power of θ-RbM' [M'=Co,Zn] and α''-ET$_2$K$_{1.4}$(SCN)$_4$, magnetic properties of θ-MZn [M=Rb,Cs] measured by a SQUID magnetometer, and pressure dependence of electrical resistivity are presented. In addition, the systematic change of the metal-insulator transition temperatures and the variety of the ground states are interpreted in view of a single phase

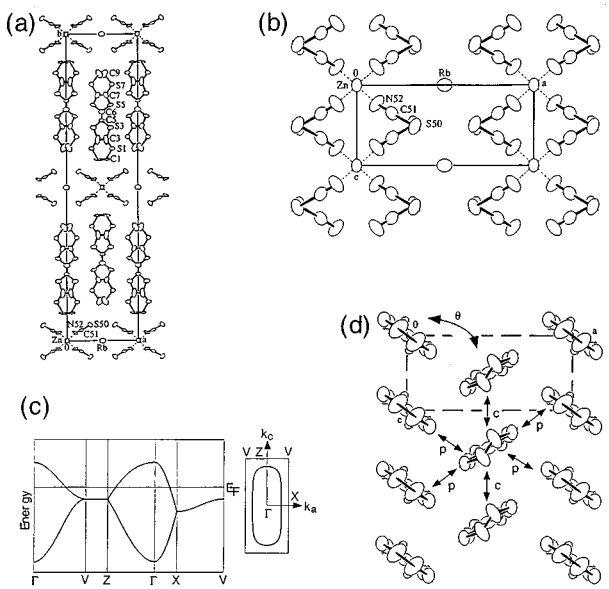

FIG. 1. (a) Crystal structure, (b) anion arrangement, (c) band structure, (d) donor arrangement of θ-(BEDT-TTF)$_2$RbZn(SCN)$_4$.

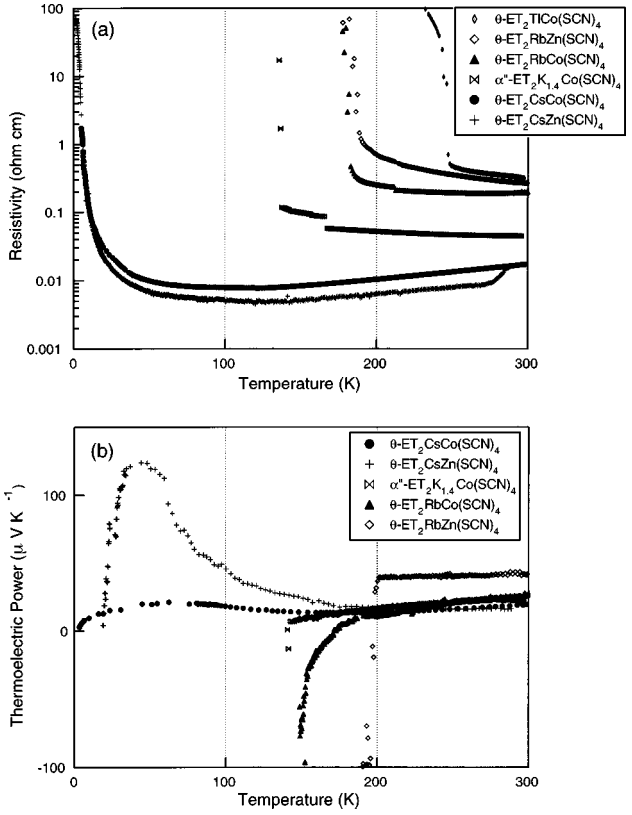

FIG. 2. Temperature dependence of (a) electrical resistivity and (b) thermoelectric power for θ-(BEDT-TTF)$_2MM'$(SCN)$_4$ [M = Tl,Rb,Cs, M' = Co,Zn] and α''-(BEDT-TTF)$_2$K$_{1.4}$Co(SCN)$_4$.

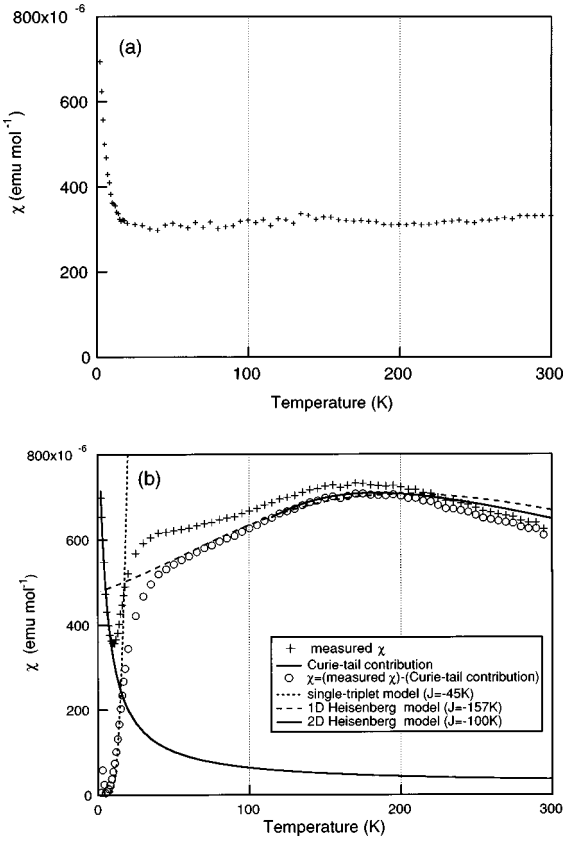

FIG. 3. Temperature dependence of magnetic susceptibility for (a) θ-(BEDT-TTF)$_2$CsZn(SCN)$_4$ and (b) θ-(BEDT-TTF)$_2$RbZn(SCN)$_4$.

diagram where U/t or the dihedral angle[6(h)] scales the properties.

EXPERIMENT

Single crystals were obtained by galvanostatic anodic oxidation of BEDT-TTF (30 mg) in a N_2 atmosphere, using the electrolyte as MSCN [M = Tl,Rb,Cs] (220 mg), M'(SCN)$_2$ [M' = Co,Zn] (120 mg), 18-crown-6 ether (205 mg) in 1,1,2-trichloroethane (90 ml) and 10% vol. of ethanol (10 ml) at a constant current of 0.5 μA.

The electrical resistivity was measured by a conventional four-probe method by applying a low ac current of 60 Hz. Gold wires (Furuya Kinzoku, 25 μmϕ) were attached to a crystal with gold paste (Tokuriki Chemicals, No. 8560) as electrodes. The resistivity under pressure was measured by using a pressure cell of clamp type with an oil (Daphne no. 7373) as a pressure medium. The pressure was determined by measuring the resistance of a manganin wire at room temperature and T_c of Sn at low temperature. Thermoelectric power was measured by attaching a single crystal to two copper heat blocks with gold paint. The heat blocks were alternately heated to generate a temperature gradient of about $\pm$0.5 K.

Magnetic susceptibility was measured by a SQUID magnetometer (Quantum Design Model MPMS7). The core contribution of components was subtracted by using Pascal's law.[7]

RESULTS AND DISCUSSION

Recently we have prepared new θ-type BEDT-TTF salts, θ-ET$_2MM'$(SCN)$_4$ [M = Tl,Rb,Cs, M' = Co,Zn: abbreviated as θ-MM'],[4(e),4(f),6] which undergo metal-insulator transitions at 250 K (θ-TlCo), 190 K (θ-RbM'; M' = Co,Zn), and 20 K (θ-CsM'; M' = Co,Zn),[4(e),4(f),6(a)–6(d)] respectively, as shown in Fig. 2(a). The metal-insulator transition temperature strongly depends upon M, where the smaller M salt gives rise to the higher transition temperature. We shall call this behavior the chemical pressure effect.

Figure 2(b) shows the temperature dependence of thermoelectric power. The values at room temperature of θ-RbM' [M' = Co,Zn] are about +23 and 42 μV/K, which are a little higher than those of θ-CsM' [M' = Co,Zn], +19 and 16 μV/K.[6(e)] The positive value indicates that the carriers are holes and the larger value shows the higher electronic correlation in θ-RbM' [M' = Co,Zn] compared with θ-CsM' [M' = Co,Zn]. With lowering temperature, thermopower of θ-RbM' [M' = Co,Zn] decreases gradually with a T linear dependence, suggesting normal metal behavior. At the metal-insulator transition temperature, 190 K, thermopower of θ-RbZn drops suddenly and that of θ-RbCo decreases gradually with crossing zero, which is in good agreement with the resistivity measurement. The thermopower of α''-KCo at room temperature is +30 μV, decreases linearly to 140 K, and diverges to the negative region, which is consistent with the metal-insulator transition at 130 K of the resistivity measurement.

In order to investigate the origin of the metal-insulator

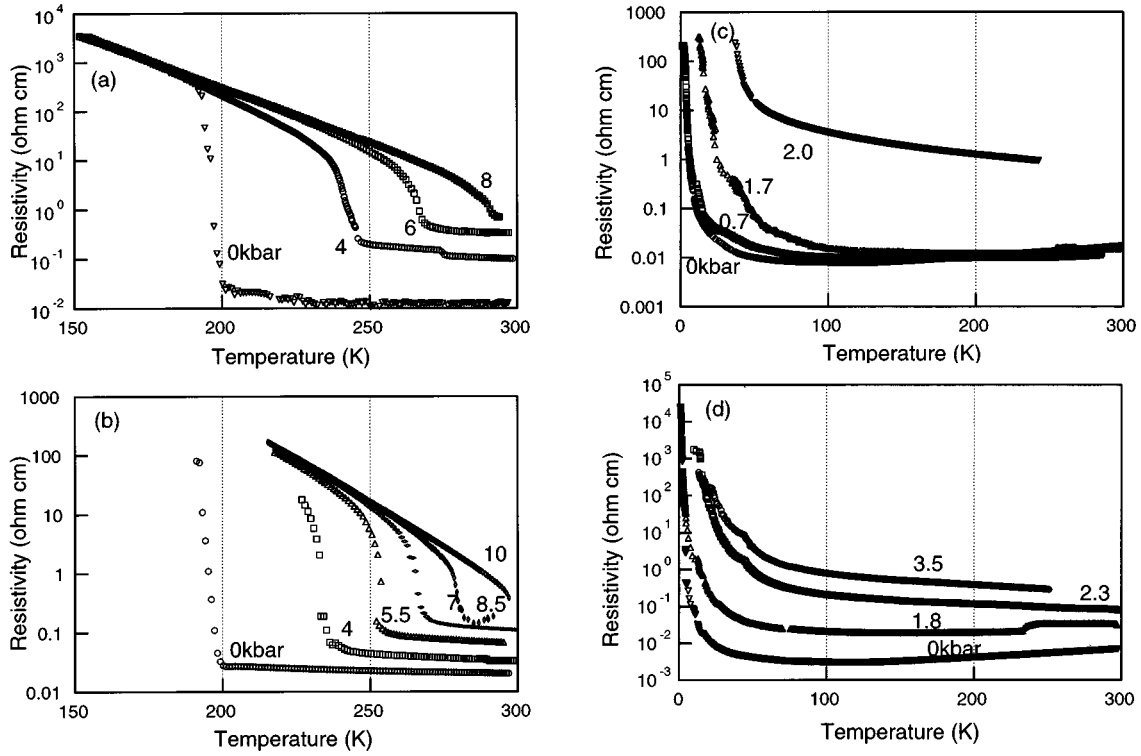

FIG. 4. Temperature dependence of electrical resistivity under pressure for θ-(BEDT-TTF)$_2MM'$(SCN)$_4$ [MM' = (a) RbCo, (b) RbZn, (c) CsCo, and (d) CsZn].

transition, the magnetic susceptibility measurements were carried out by a SQUID magnetometer with using the unoriented powder sample. The susceptibility at room temperature for θ-CsZn is 3.3×10^{-4} emu mol^{-1}, which is the typical value of Pauli paramagnetism of an organic conductor: for example, 4.6×10^{-4} emu mol^{-1} in κ-ET$_2$Cu(NCS)$_2$.[8] The susceptibility is almost constant down to 20 K and below that temperature a Curie-tail contribution is observed, so the origin of the metal-insulator transition at 20 K is not clear [Fig. 3(a)]. On the other hand, the susceptibility of θ-RbZn, from which a Curie-tail contribution has been subtracted, is shown in Fig. 3(b). The broken line is the calculated susceptibility based upon the one-dimensional Heisenberg antiferromagnet (Bonner-Fisher model[9]) with $J=-157$ K and the solid line is that on the two-dimensional quadratic-layer Heisenberg antiferromagnet[10] with $J=-100$ K. In both cases, the measured susceptibility is smaller than the models from room temperature to 190 K, the metal-insulator transition temperature, suggesting that electrons are less localized in this temperature region. The crystal structure analysis shows that the room-temperature regular stacking of donors undergoes a lattice modulation at 190 K, where the sudden appearance of $c^*/2$ is observed.[4(f)] Then, the carriers are located below 190 K. This structural transition induces no abrupt change of magnetic susceptibility, which indicates that the system is highly correlated even above the transition temperature. Below 190 K the measured susceptibility follows the Heisenberg model down to 50 K. With lowering temperature further, susceptibility decreases rapidly, where the behavior can be fitted by the singlet-triplet model with $J=-45$ K at lower temperatures, indicating that the spin singlet state is realized. Recently the long-range-order-like spin Peierls state has been observed by NMR measurement.[6(i)]

In order to suppress this metal-insulator transition, an external pressure is applied in this system. The temperature dependence of resistance at various pressures is illustrated in Figs. 4(a)–4(d) for θ-RbCo, θ-RbZn, θ-CsCo, and θ-CsZn, respectively. The metal-insulator transition temperatures, corresponding to the rapid increase or the kink in the temperature dependence, are elevated with applying pressure for these salts, so we shall call this phenomenon a pressure-induced metal-insulator transition. A phase diagram under external pressure is shown in Fig. 5. Though the pressure dependence of θ-RbZn (or θ-CsZn) is a little smaller than that of θ-RbCo (or θ-CsCo), four salts have almost the same pressure dependence. This inverse pressure dependence is observed not only (i) when external pressure but also (ii) when chemical pressure is applied or (iii) when temperature

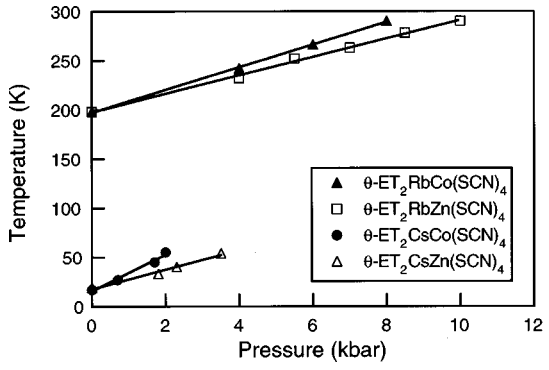

FIG. 5. Phase diagram of metal-insulator transition temperature under pressure.

TABLE I. The lattice parameters, dihedral angle, unit cell ratio, transfer integral in the transverse direction (t_p), and calculated bandwidth of θ-$ET_2MM'(SCN)_4$ [M=Tl,Rb,Cs, M'=Zn,Co].

	θ-$(ET)_2TlCo(SCN)_4$	θ-$(ET)_2RbCo(SCN)_4$ (300 K)	θ-$(ET)_2RbCo(SCN)_4$ (7 K)
system	orthorhombic	orthorhombic	monoclinic
space group	$I222$	$I222$	$C2$
a/Å	10.393(7)	10.176(6)	43.31(1)
b/Å	43.16(1)	43.258(4)	10.311(2)
c/Å	4.50(1)	4.650(5)	8.905(3)
α/deg	90	90	90
β/deg	90	90	95.81(2)
γ/deg	90	90	90
V/Å^3	2017(5)	2047(2)	3955(1)
dihedral angle/deg	116	111	114
unit cell ratio a/c	2.31	2.19	
unit cell ratio $b/(c/2)$			2.32
transfer integral in the transverse direction/$\times 10^{-2}$ eV	−10.0	−9.9	8.2–14.4
bandwidth/eV	0.82	0.82	0.90
reference	4f	4f,6b	4f
	θ-$(ET)_2RbZn(SCN)_4$	θ-$(ET)_2CsCo(SCN)_4$	θ-$(ET)_2CsZn(SCN)_4$
system	orthorhombic	orthorhombic	orthorhombic
space group	$I222$	$I222$	$I222$
a/Å	10.175(9)	9.804(4)	9.816(4)
b/Å	43.301(9)	43.416(3)	43.443(5)
c/Å	4.65(1)	4.873(4)	4.870(4)
α/deg	90	90	90
β/deg	90	90	90
γ/deg	90	90	90
V/Å^3	2047(5)	2074(3)	2077(2)
dihedral angle/deg	111	104	105
unit cell ratio a/c	2.19	2.01	2.02
transfer integral in the transverse direction/$\times 10^{-2}$ eV	−9.4	−10.6	−10.8
bandwidth/eV	0.78	0.86	0.88
reference	4f,6b	4e,6a	4e,6a

is lowered. When the chemical pressure is applied by changing the cation like Cs^+ [2077(2) Å^3 (θ-CsZn) and 2074(3) (θ-CsCo)]>Rb^+ [2047(5) (θ-RbZn) and 2047(2) (θ-RbCo)]>Tl^+ [2017(5) (θ-TlCo)], the metal-insulator transition temperature increases like 20<190<250 K. At the same time, the c axis contracts like 4.870(4) Å (θ-CsZn) and 4.873(4) (θ-CsCo)>4.65(1) (θ-RbZn) and 4.650(5) (θ-RbCo)>4.50(1) (θ-TlCo), while the a axis expands like 9.816(4) Å (θ-CsZn) and 9.804(4) (θ-CsCo)<10.175(9) (θ-RbZn) and 10.176(6) (θ-RbCo)<10.393(7) (θ-TlCo) (Table I, Fig. 6). This chemical pressure behavior is schematically illustrated in Fig. 7. Changing from (a) to (b) by applying pressure, c decreases and a increases, resulting in increasing the dihedral angle between donor columns like 105° (θ-CsZn) and 104° (θ-CsCo)<111 (θ-RbZn) and 111 (θ-RbCo)<116 (θ-TlCo) and the unit cell ratio, a/c, like 2.02 (θ-CsZn) and 2.01 (θ-CsCo)<2.19 (θ-RbZn) and 2.19 (θ-RbCo)<2.31 (θ-TlCo). Moreover, the calculated transfer integral in the transverse direction (t_p), which determines the bandwidth (W) in this system, decreases like $|t_p|$=10.8 ($\times 10^{-2}$ eV) (θ-CsZn) and 10.6 (θ-CsCo)>9.4 (θ-RbZn) and 9.9 (θ-RbCo)~10.0 (θ-TlCo). In the θ-type salts the intracolumnar interaction t_c is much smaller than t_p, so the overall bandwidth W is principally determined by t_p. Then, W decreases like W=0.88 (eV) (θ-CsZn) and 0.86 (θ-CsCo)>0.78 (θ-RbZn) and 0.82 (θ-RbCo)~0.82 (θ-TlCo) (Table I, Fig. 6). Since U is the characteristic value of the donor molecule and is all the same in the θ-type BEDT-TTF salts, the electronic correlation parameter, U/t, increases with decreasing transfer integral (t) or with increasing dihedral angle of donors and makes the metal-insulator (MI) transition temperature (T_{MI}) higher. This is why the pressure-induced metal-insulator transition occurs when chemical pressure is applied. Strictly speaking, the transition of θ-CsM' is different from those of θ-RbM' and θ-TlCo. Though the unit cell volume decreases from θ-CsM', θ-RbM', to θ-TlCo with regular intervals of about 30 Å^3, the metal-insulator transition temperature is elevated from 20

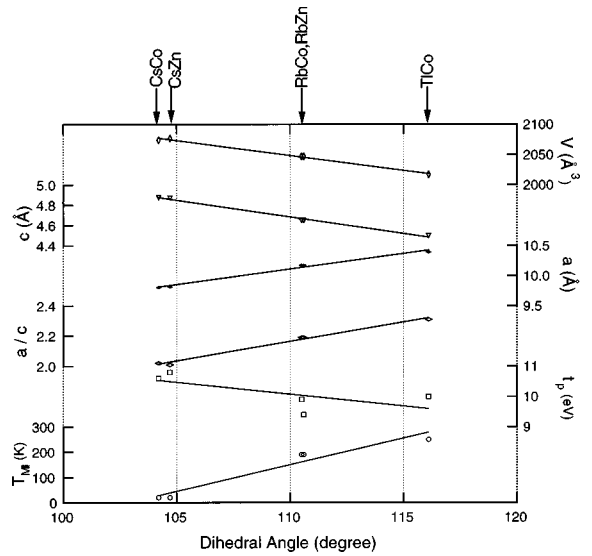

FIG. 6. Dihedral angle dependence of the unit cell volume (V), the c-axis (c), the a-axis (a), the unit cell ratio (a/c), the transfer integral along the transverse direction (t_p), and the metal-insulator transition temperature (T_{MI}) for θ-(BEDT-TTF)$_2MM'$(SCN)$_4$ [MM'=CsCo, CsZn, RbCo, RbZn, and TlCo].

K (θ-CsM'), 190 K (θ-RbM'), to 250 K (θ-TlCo); the increases are not equivalent. The transitions of θ-RbM' and θ-TlCo are related to the lattice modulation at the transition temperature. Investigations of temperature dependence of the lattice constants show that the dihedral angle and the unit cell ratio for θ-RbM' increase abruptly at the transition, leading to a sudden increase of electronic correlation at that temperature.[4(f)] By lowering temperature as well as chemical pressure, the dihedral angle and the unit cell ratio for θ-RbCo increase from 111°, 2.19 (300 K) to 114°, 2.32 (7 K) as shown in Table I. When the bandwidth is reduced in comparison with the on-site Coulomb repulsion by decreasing temperature, the metal-insulator transition is induced. The same behavior happens when the external pressure is applied.

The phase diagram for θ-type BEDT-TTF salts is shown in Fig. 8, where the observed transition temperature is plotted as a function of the dihedral angle of donor columns, θ, and the calculated transfer integral, t.[11] As discussed above, an increase of the dihedral angle, θ, leads to a significant decrease of transfer integral in the transverse direction, t, that is to say, an increase of U/t. On the right end of the phase diagram the superconducting phase, θ-ET_2I_3,[5] exists, while on the left end, insulators are present such as θ-$ET_4Hg_3I_8$,[4(a)] $ET_2Cu_2(CN)[N(CN)_2]_2$,[4(b)] $ETAgBr_3$,[4(c)]

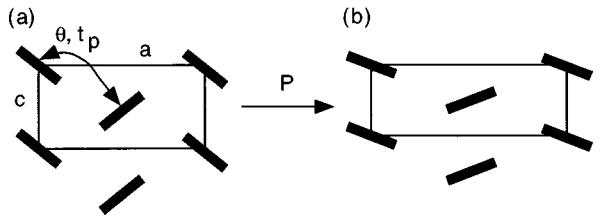

FIG. 7. Scheme for pressure effect of donors in θ-(BEDT-TTF)$_2MM'$(SCN)$_4$ [M=Rb,Cs, M'=Co,Zn].

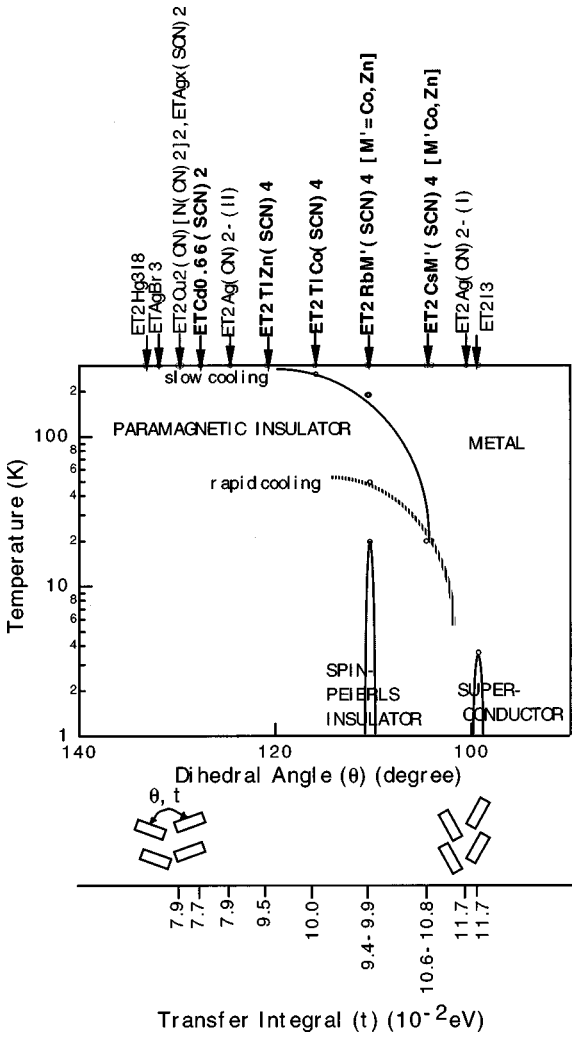

FIG. 8. Phase diagram for θ-type BEDT-TTF salts as a function of a transfer integral in the transverse direction (t) and a dihedral angle of donor columns (θ).

$ETAg_x(SCN)_2$,[4(d)] and $ETCd_{0.66}(SCN)_2$.[4(e)] The first two θ-ET salts have been confirmed to be paramagnetic insulators. We have prepared the series θ-MM' [M=Tl,Rb,Cs, M'=Co,Zn], which is located between the superconducting and insulating phases. For θ-RbM' [M'=Co,Zn], they are in a metallic phase at room temperature, below 190 K they lose the metallic character to become a paramagnetic insulator, and the singlet state is observed at low temperatures.

Nakamura *et al.* reported that the temperature dependence of the magnetic susceptibility for θ-RbM' (M'=Co,Zn) strongly depends upon the cooling speed.[6(g)] With cooling a sample slowly (0.8 K/min), magnetic susceptibility follows the Heisenberg model below the metal-insulator transition temperature, 190 K, and decreases rapidly as fitted by a single-triplet model with $J=-45$ K below 40 K [Fig. 3(b)].[6(c)] In addition, the Curie-tail contribution is observed at low temperatures. By cooling a sample more rapidly (10 K/min), the Curie-tail contribution increases, and in the rapid cooling condition the magnetic susceptibility follows the Curie-Weiss law at low temperatures without a sudden decrease below 40 K. Since the complete lattice modulation is not performed in the rapid cooling condition, the singlet state cannot be obtained at low temperatures. Therefore, the

metal-insulator transition temperature is lowered in the rapid cooling condition due to the imperfect lattice modulation, and then the ground state might be different from that in the slow cooling condition. In the NMR measurement of θ-RbZn in the rapid cooling condition, the sudden increase of T_1^{-1}, suggesting the antiferromagnetic fluctuation, has been observed at 50 K, whose behavior resembles that of θ-CsZn at 20 K. This observation makes us assume that the metal-insulator transition of θ-CsZn at 20 K should not be directly related to that of θ-RbZn at 190 K in nature, but rather related to the magnetic anomaly of θ-RbZn at 50 K under the rapid cooling condition. Thus, the dotted line in the rapid cooling condition as shown in Fig. 8 is connected from 50 K of θ-RbZn to 20 K of θ-CsZn.[6(g)] Moreover, the mixed crystal of θ-(Rb+Cs)Zn is recently prepared and the preliminary result indicates that the metal-insulator transition temperature is on the dotted line owing to the failure of lattice modulation. The transition depicted by the dotted line without structural transition seems to be mainly driven by the intrinsic electronic correlation, while the transition illustrated as a solid line is related to the lattice modulation, which induces the electronic correlated state. In the extension of the solid and dotted lines, there exists a superconducting state in the θ-ET phase diagram. Further study will be reported in a separate paper.[12]

Finally, we describe a noticeable point in the phase diagram. As shown in Fig. 8, the behavior of the phase transitions in the θ-ET family is mapped out as a function of the electronic correlation parameter, U/t. This behavior is similar to that of the κ-ET family, which are two-dimensional organic conductors. In the κ-phase diagram, four phases—paramagnetic metal, paramagnetic insulator, superconductor, and antiferromagnetic insulator—exist and their electronic states are also scaled by the electronic correlation parameter, U/W, where U is the effective on-site Coulomb energy and W is the bandwidth.[13] The metal-nonmetal transition in the κ phase is driven by electronic correlation, whereas the transition in the θ phase is related to not only the electronic correlation in nature, but also the lattice modulation; the structural transition occurs, resulting in the localized spin below the transition temperature constructing the electronic correlated state, namely, the paramagnetic insulator. The ground states of the paramagnetic insulators could be the antiferromagnetic-state-like κ-ET family or the spin-Peierls state like TMTTF family. The ground states in the θ-ET family seem to depend upon cooling speed. In the slow cooling, the behavior of magnetic susceptibility indicates the coexistence of the Curie contribution and the term fitted by the singlet-triplet model below 50 K, suggesting that the ground state is the spin-Peierls state. In the rapid cooling condition, only the Curie contribution is observed and the ground state might be the antiferromagnetic state. It is important to investigate the ground states of paramagnetic insulators in the vicinity of the superconducting state in the θ-ET family.

In conclusion, the behavior of the phase transition is mapped out for θ-BEDT-TTF salts including θ-(BEDT-TTF)$_2MM'$(SCN)$_4$ [M=Tl,Rb,Cs, M'=Co,Zn], which we have recently prepared, as a function of dihedral angle, θ, or transfer integral, t, between donor columns. The electronic correlation parameter (U/t) increases by increasing a dihedral angle, θ. The ground state of θ-BEDT-TTF salts varies from insulating, superconducting, to metallic state with decreasing θ, namely, U/t. The series θ-MM' is located at the center of the phase diagram where metallic, paramagnetic insulating, and singlet states are obtained at low temperatures. The change of electronic state in the increase of θ, in other words, U/t, is observed not only by the chemical pressure effect from θ-CsM', θ-RbM', to θ-TlCo and the decrease of temperature, but also by the external pressure. With applying pressure for θ-MM', the metal-insulator transition temperature increases, which is related to the enhancement of the electronic correlation. It is important to investigate the ground state of the paramagnetic insulator of θ-ET$_2MM'$(SCN)$_4$ [M=Tl,Rb,Cs, M'=Co,Zn] in the vicinity of an organic superconducting state.

ACKNOWLEDGMENTS

The authors wish to thank Dr. T. Nakamura and Professor T. Takahashi of Gakushuin University and Professor I. Terasaki of Waseda University for fruitful discussions, and express their gratitude to Professor A. Kobayashi and Professor H. Kobayashi for their kind offer of the atomic coordinate of θ-(BEDT-TTF)$_2$I$_3$.

[1] (a) T. Mori, A. Kobayashi, Y. Sasaki, H. Kobayashi, G. Saito, and H. Inokochi, Bull. Chem. Soc. Jpn. **57**, 627 (1984). The extended Huckel calculation is carried out with a basis set of Slater orbital of single-ξ quality. The exponents and parameters used are therein. (b) M.-H. Whangbo, J. M. Williams, P. C. W. Leung, M. A. Beno, T. J. Emge, H. H. Wang, K. D. Carlson, and G. W. Crabtree, J. Am. Chem. Soc. **107**, 5815 (1985). (c) E. Canadell, I. E.-I. Rachidi, S. Ravy, J. P. Pouget, L. Brossard, and J. P. Legros, J. Phys. (France) **50**, 2967 (1989).

[2] K. Oshima, T. Mori, H. Inokuchi, H. Urayama, H. Yamochi, and G. Saito, Phys. Rev. B **38**, 938 (1988); recent review is given in J. Wosnitza, Int. J. Mod. Phys. B **7**, 2707 (1993); J. Wosnitza, *Fermi Surfaces of Low-Dimensional Organic Metals and Superconductors* (Springer, Berlin, 1996); K. Yamaji, J. Phys. Soc. Jpn. **58**, 1520 (1989).

[3] (a) M. A. Beno, M. A. Firestone, P. C. W. Leung, L. M. Sowa, H. H. Wang, J. M. Williams, and M.-H. Whangbo, Solid State Commun. **57**, 735 (1986). (b) H. Kobayashi, R. Kato, A. Kobayashi, G. Saito, M. Tokumoto, H. Anzai, and T. Ishiguro, Chem. Lett. **1986**, 89 (1986); T. J. Emge, H. H. Wang, P. C. W. Leung, P. R. Rust, J. D. Cook, P. L. Jackson, K. D. Carlson, J. M. Williams, M.-H. Whangbo, E. L. Venturini, J. E. Schirber, L. J. Azevedo, and J. R. Ferraro, J. Am. Chem. Soc. **108**, 695 (1986). (c) U. Geiser, H. H. Wang, M. A. Beno, M. A. Firestone, K. S. Webb, and J. M. Williams, Solid State Commun. **57**, 741 (1986).

[4] (a) T. G. Takhirov, O. N. Krasochka, O. A. Dyachenko, L. O. Atovmyan, M. Z. Aldoshina, L. M. Goldenberg, R. N. Lyubovskaya, V. A. Merzhanov, and R. B. Lyunovskii, Mol. Cryst. Liq. Cryst. **185**, 215 (1990). (b) T. Komatsu, H. Sato, T. Naka-

mura, N. Matsukawa, H. Yamochi, G. Saito, M. Kusunoki, K. Sakaguchi, and S. Kagoshima, Bull. Chem. Soc. Jpn. **68**, 2233 (1995). (c) U. Geiser, H. H. Wang, P. R. Rust, L. M. Tonge, and J. M. Williams, Mol. Cryst. Liq. Cryst. **181**, 117 (1990). (d) U. Geiser, M. A. Beno, A. M. Kini, H. H. Wang, A. J. Schultz, B. D. Gates, C. S. Cariss, J. D. Carlson, and J. M. Williams, Synth. Met. **27**, A235 (1988). (e) H. Mori, S. Tanaka, T. Mori, and Y. Maruyama, Bull. Chem. Soc. Jpn. **68**, 1136 (1995). (f) H. Mori *et al.*, *ibid.* (to be published).

[5] H. Kobayashi, R. Kato, A. Kobayashi, Y. Nishio, K. Kajita, and W. Sasaki, Chem. Lett. **1986**, 789 (1986); **1986**, 833 (1986).

[6] (a) H. Mori, I. Hirabayashi, S. Tanaka, T. Mori, and Y. Maruyama, Synth. Met. **70**, 789 (1995). (b) H. Mori, S. Tanaka, and T. Mori, Mol. Cryst. Liq. Cryst. Sci. Technol., Sect. A **284**, 15 (1996). (c) H. Mori, S. Tanaka, T. Mori, and A. Fuse, Synth. Met. **86**, 1789 (1997). (d) H. Mori, S. Tanaka, and T. Mori, J. Phys. I **6**, 1987 (1996). (e) T. Mori, A. Fuse, H. Mori, and S. Tanaka, Physica C **264**, 22 (1996). (f) T. Nakamura, R. Kinami, W. Minagawa, T. Takahashi, H. Mori, S. Tanaka, and T. Mori, Mol. Cryst. Liq. Cryst. Sci. Technol., Sect. A **285**, 57 (1996). (g) T. Nakamura *et al.*, in *Meeting Abstracts of the Physical Society of Japan, March, 1996* (Physical Society of Japan, Tokyo, 1996). (h) The dihedral angle is determined by two least square planes of donor molecules as shown in Fig. 1(d). The plane is defined as the central tetrathio-substituted ethylene moiety of the BEDT-TTF molecule. (i) T. Nakamura (private communication).

[7] *Kagaku Binran, Kisohen II* (Maruzen, Tokyo, 1989), Ver. 3, p. II-508.

[8] K. Nozawa, T. Sugano, H. Urayama, H. Yamochi, G. Saito, and M. Kinoshita, Chem. Lett. **1988**, 617 (1988).

[9] J. C. Bonner and M. E. Fisher, Phys. Rev. **135**, A640 (1964); W. E. Hatfield, W. E. Estes, W. E. Marsh, M. W. Pickens, L. W. ter Haar, and R. R. Weller, in *Extended Linear Chain Compounds*, edited by J. S. Miller (Plenum, New York, 1983), Vol. 3, Chap. 2, p. 45.

[10] L. J. deJongh, in *Magnetism and Magnetic Materials–1972*, edited by C. D. Graham and J. Phyne, AIP Conf. Proc. No. 10 (American Institute of Physics, New York, 1973), p. 561; G. S. Rushbrooke and P. J. Wood, Mol. Phys. **1**, 257 (1958); M. E. Lines, J. Phys. Chem. Solids **31**, 101 (1970).

[11] The transfer integrals of θ-BEDT-TTF salts in Fig. 8 are recalculated by using our own parameters (Ref.1).

[12] H. Mori *et al.* (unpublished).

[13] K. Kanoda, Hyperfine Interact. **104**, 235 (1997).